

UC Berkeley

UC Berkeley Previously Published Works

Title

Comparing Theoretical Salt Concentration Profiles in a Polymer Electrolyte with Experimental Measurements using Operando Raman Spectroscopy

Permalink

<https://escholarship.org/uc/item/35m451r1>

Journal

Journal of The Electrochemical Society, 170(9)

ISSN

0013-4651

Authors

Hoffman, Zach J
Galluzzo, Michael D
Gordon, Madeleine P
et al.

Publication Date

2023-09-01

DOI

10.1149/1945-7111/acf626

Copyright Information

This work is made available under the terms of a Creative Commons Attribution License, available at <https://creativecommons.org/licenses/by/4.0/>

Peer reviewed

OPEN ACCESS

Comparing Theoretical Salt Concentration Profiles in a Polymer Electrolyte with Experimental Measurements using *Operando* Raman Spectroscopy

To cite this article: Zach J. Hoffman *et al* 2023 *J. Electrochem. Soc.* **170** 090517

View the [article online](#) for updates and enhancements.

You may also like

- [Effect of Solvent Motion on Ion Transport in Electrolytes](#)
Aashutosh Mistry, Lorena S. Grundy, David M. Halat *et al.*
- [Comparing Two Electrochemical Approaches for Measuring Transference Numbers in Concentrated Electrolytes](#)
Danielle M. Pesko, Simar Sawhney, John Newman *et al.*
- [Negative Stefan-Maxwell Diffusion Coefficients and Complete Electrochemical Transport Characterization of Homopolymer and Block Copolymer Electrolytes](#)
Irene Villaluenga, Danielle M. Pesko, Ksenia Timachova *et al.*



We Advance Battery Research!

- Electrochemical Battery Test Cells
- Multi-channel Potentiostats / Galvanostats / EIS
- Tools, Consumables & Testing Services

el-cell.com

+49 40 79012-734

sales@el-cell.com


electrochemical test equipment





Comparing Theoretical Salt Concentration Profiles in a Polymer Electrolyte with Experimental Measurements using *Operando* Raman Spectroscopy

Zach J. Hoffman,^{1,2,3}  Michael D. Galluzzo,^{1,2}  Madeleine P. Gordon,⁴ 
Jeffrey J. Urban,⁴  and Nitash P. Balsara^{1,2,3,5,z} 

¹Department of Chemical and Biomolecular Engineering, University of California, Berkeley, Berkeley, California 94720, United States of America

²Materials Sciences Division, Lawrence Berkeley National Laboratory, Berkeley, California 94720, United States of America

³Joint Center for Energy Storage Research (JCESR), Lawrence Berkeley National Laboratory, Berkeley, California 94720, United States of America

⁴Molecular Foundry, Lawrence Berkeley National Laboratory, Berkeley, CA 94720, United States of America

⁵Energy Storage and Distributed Resources Division, Lawrence Berkeley National Laboratory, Berkeley, CA 94720, United States of America

Concentrated solution theory has furthered our understanding of ion transport in electrolytes. This theory can be used to predict salt concentration profiles under an applied current if the transport properties of the electrolyte (conductivity (κ), restricted diffusion coefficient (D), and the cation transference number with respect to the solvent velocity (t_+^0)), and the thermodynamic factor (T_f) are known. In this work, we provide the first study comparing the predicted salt concentration profiles with measurements based on *operando* Raman spectroscopy. Concentration polarization is asymmetrical; the increase in salt concentration near the positive electrode is a factor of two greater than the decrease in salt concentration near the negative electrode. We find qualitative agreement between theory and experiment. Further work is needed to resolve the quantitative differences.

© 2023 The Author(s). Published on behalf of The Electrochemical Society by IOP Publishing Limited. This is an open access article distributed under the terms of the Creative Commons Attribution 4.0 License (CC BY, <http://creativecommons.org/licenses/by/4.0/>), which permits unrestricted reuse of the work in any medium, provided the original work is properly cited. [DOI: 10.1149/1945-7111/acf626]



Manuscript submitted March 17, 2023; revised manuscript received July 28, 2023. Published September 13, 2023.

Supplementary material for this article is available [online](#)

List of Symbols

Symbol	Description
A_n	Normalized area of PEO and Anion Raman peaks
c	Molar salt concentration, mol/L
D_{dU}	Restricted diffusion coefficient, cm ² /sec
$\frac{dU}{d \ln m}$	Change in open circuit potential with respect to the natural log of molality
F	Faraday constant, C/mol
r	Salt Concentration ($r = [\text{Li}^+]/[\text{EO}]$)
r_{avg}	Average salt concentration
r_{exp}	Experimentally measured salt concentration
r_{theory}	Salt concentration predicted from theory
t_+^0	Cationic transference number
t_-^0	Anionic transference number
T_f	Thermodynamic Factor
v_+	Number of cations
x/L	Normalized distance across the electrolyte
z_+	Charge of cation
δr	Difference between calculated and expected r_{avg}
Δr	Difference between predicted and experimentally measured salt concentration
κ	Ionic conductivity, S/cm
ρ_+	Current fraction

There is great interest in replacing the conventional rechargeable battery electrolytes, mixtures of organic solvents and a metal salt, for the next generation of rechargeable batteries. These electrolytes provide superior performance; however their flammability provides significant safety concerns, and they are unstable against high capacity electrodes such as lithium metal.¹⁻³ Additionally, these

liquid electrolytes provide no physical resistance to the growth of lithium dendrites which can grow under fast charging conditions and lead to catastrophic failure.⁴⁻⁶ Polymer electrolytes have the potential to address some of the limitations of liquid electrolytes.⁷

When current is drawn across an electrolyte, salt concentration gradients will develop, resulting in depletion of salt at the negative electrode and accumulation of salt at the positive electrode.⁸ These salt concentration gradients limit cell safety and performance. Theoretical models suggest that the propensity for lithium dendrite growth is accentuated by large salt concentration gradients.⁹ The fastest rate of charging a cell is determined by the magnitude of salt concentration gradients. As larger values of current are drawn across the cell, these gradients grow. At a sufficiently large current, the salt concentration throughout the negative electrode is zero (or nearly so); this is defined to be the limiting current of the electrolyte. Drawing currents larger than the limiting current will result in decomposition of the electrolyte and failure of the cell.

The salt concentration profile through an electrolyte at a given current density, i , can be calculated using concentrated solution theory.^{10,11} This calculation requires knowledge of three transport parameters, conductivity (κ), restricted diffusion coefficient (D), and the cationic transference number (t_+^0), along with the thermodynamic factor (T_f).^{12,13} While κ can be measured by simple ac impedance experiments,¹⁴⁻¹⁶ determining the other 3 parameters requires considerable effort. However, the performance of an electrolyte in a cell can only be predicted if all four parameters are known as a function of salt concentration.

Predictions based on concentrated solution theory have been used to explore the underpinnings of cell cycling data in several cases.^{10,11,17} In typical experiments, the potential drop across the cell is measured as a function of current density. These measurements may be considered as indirect reporters of salt concentration gradients. Salt concentration gradients have been measured directly via Raman spectroscopy in some electrolytes.¹⁸⁻²³ The work in Ref. 18 is particularly noteworthy as they

^zE-mail: nbalsara@berkeley.edu

use the measured concentration gradient to determine transport properties and the thermodynamic factor. There are, however, no studies wherein the measured concentration gradient is compared with the predictions of concentrated solution theory without resorting to adjustable parameters. In this work we use *operando* Raman spectroscopy to determine the salt concentration profile in a polymer electrolyte at a fixed current density. The measured profiles are compared with predictions based on concentrated solution theory with no adjustable parameters.

Experimental Methods

Electrolyte preparation.—Poly(ethylene oxide) (PEO) with a molecular weight of 275 kg mol^{-1} (Polymer Source) and Lithium bis(trifluoromethanesulfonyl)imide (LiTFSI) (Sigma Aldrich) were dried under active evacuation for three days at 120°C . They were then combined and dissolved in anhydrous tetrahydrofuran (THF) (Sigma Aldrich) at 60°C in a capped vial, and then once dissolved, the cap is removed to evaporate off the THF. The electrolytes were then dried at 90°C under active evacuation for a day to remove any remaining solvent. Preparation of electrolytes was performed in an

argon-filled glovebox with water levels below 1 ppm and oxygen levels below 2 ppm. The electrolytes used in this study all have the same salt concentration, r , the ratio of lithium ions to ethylene oxide moieties ($r = [\text{Li}^+]/[\text{EO}]$). The r value chosen was $r = 0.08$.

Electrochemical cell preparation.—A custom electrochemical cell was developed for these experiments and is shown below in Figs. 2a–2b. Reflective tape was placed against the bottom of the cell where the electrolyte is placed to help increase the measured Raman signal. Lithium foil is then pressed against the stainless-steel electrodes and then inserted into the cell. The area of the electrode in contact with the electrolyte is 0.035 cm^2 . Then PEO/LiTFSI electrolyte is inserted between the electrodes. The channel is heated, and the electrolyte is further pressed into the channel to ensure it is filled with electrolyte. The depth of the electrolyte is 0.0875 cm , and the distance between the electrodes is 0.1 cm . The cell is then heated to 90°C and a preconditioning cycle is applied where the cell is polarized at $+10 \mu\text{A cm}^{-2}$ for four hours, allowed to relax, and then polarized at $-10 \mu\text{A cm}^{-2}$ for four hours, then allowed to relax. These polarizations were repeated three times, and ac impedance measurements were made throughout this process to track the bulk

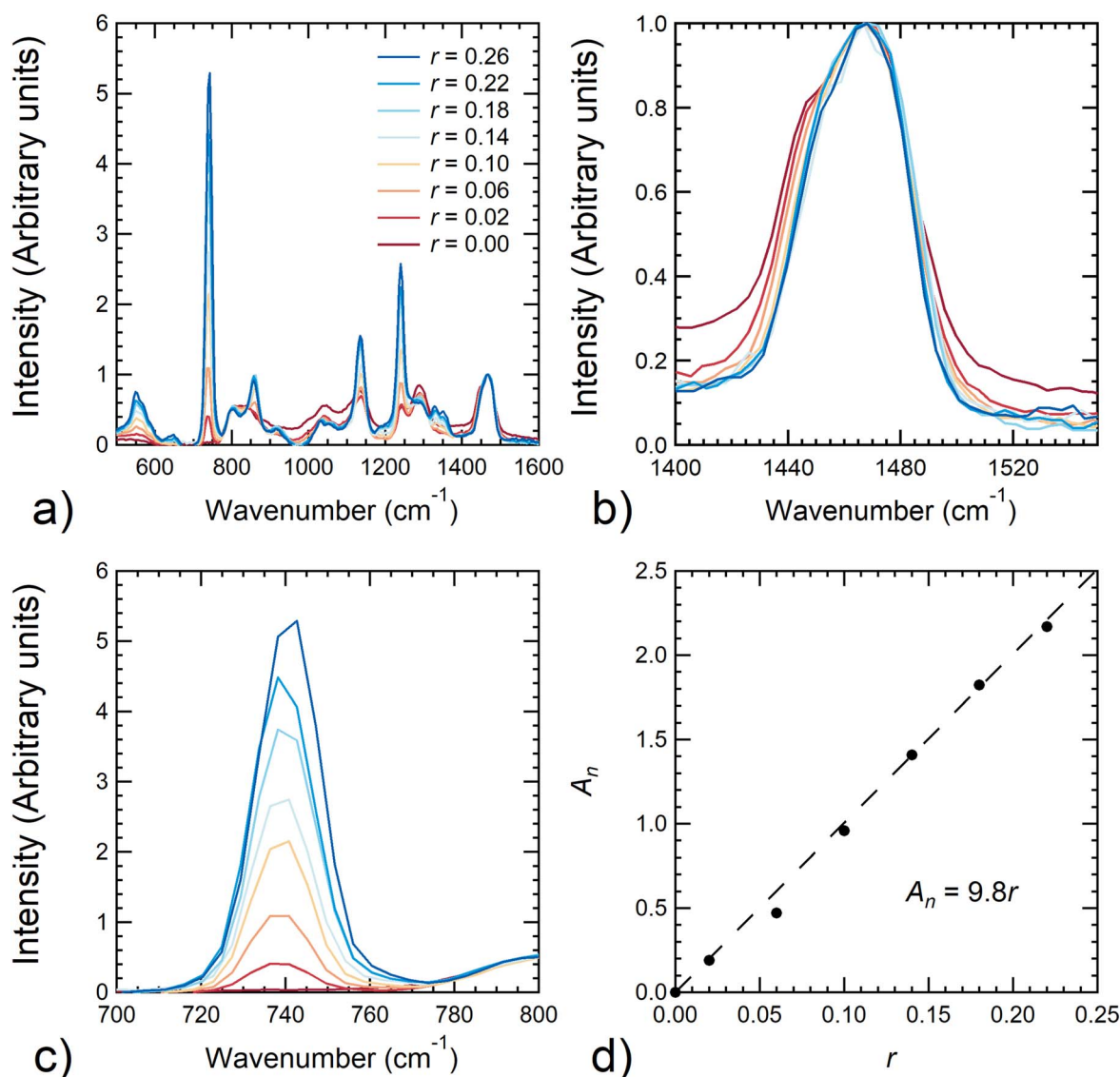


Figure 1. (a) Raman spectra of PEO/LiTFSI electrolytes with salt concentrations $0 \leq r \leq 0.26$, where $r = [\text{Li}^+]/[\text{EO}]$. Raman peaks corresponding to vibrations of (b) the PEO backbone, and (c) the TFSI⁻ anion. (d) The ratio of the fitted area of the anion peak normalized by the PEO peak, plotted as a function of r . The dashed black line represents a linear fit through the data. We use this linear fit as a calibration to determine the spatial dependence of salt concentration in the *operando* Raman cell.

and interfacial resistances. The impedance data was fit to the equivalent circuit shown in Fig. S1. All the above procedures were performed within a glovebox with less than 1 ppm levels of oxygen and water.

Polarization experiments.—After preconditioning the electrochemical cell was sealed and removed from the glovebox. The electrochemical cell was brought to the microscope and heated to 90 °C using a custom heating stage. Throughout the initial heating and polarization experiments, an argon purge stream is used to ensure that the cell is kept free of air and water. After the cell is brought to temperature, an initial ac impedance measurement is taken, along with an initial Raman scan. Afterwards the cell is polarized with an applied current density, until the measured salt concentration gradients reach steady state.

Raman measurements.—The microscope used for these experiments is a WITec alpha 300 S confocal microscope with a Raman spectrometer and a UHTS-300 CCD detector. The grating used for these experiments was 1800 grooves/mm, and the laser has a wavelength of 532 nm. A Nikon E Plan lens with 20x magnification was used to focus the laser light. For each measurement point, eight 0.6 s integrations were taken. The cell was moved during measurements using a micrometer-controlled translation stage. The cell was polarized in the x -direction (Fig. 2). The beam travels in the z -direction and thus our measurements intrinsically represent concentration averaged along this direction. Before polarization experiments, initial Raman measurements were made to identify the y value that maximized the Raman signal, relative to the background. We posit that the measured signal-to-background ratio was affected by factors such as reabsorption of Raman scattering, internal

reflection, and inhomogeneities within the cell on the scale of optical wavelengths ($0.5 \mu\text{m}$). For calibration curve measurements, simple stainless-steel air-free cells (Kurt J. Lesker Company) were utilized. Silicone spacer material was placed inside the stainless-steel cells and filled with electrolyte. These cells were then sealed before being removed from the glovebox. All the above procedures were performed within a glovebox with less than one ppm levels of oxygen and water. The cells were then brought to the Raman microscope and heated with a custom heating stage to 90 °C, at which point the Raman spectra was measured.

Results and Discussion

Previous studies have shown that Raman spectra of PEO/LiTFSI and other electrolytes are sensitive functions of salt concentration.^{18,19,22–25} Our approach builds upon these studies. In Fig. 1a the Raman spectra of PEO/LiTFSI mixtures with different salt concentrations are shown. Due to fluorescence in the measured Raman spectra, background subtraction was required for interpreting all the measured spectra. In our work, background subtraction was performed using a Python program, following the iterative approach proposed by Lieber et al.²⁶ In this study, establishing the background required about 30 iterations. Figure S2 gives an example of an original spectrum and the background. The background-subtracted spectra are shown in Fig. 1a.

We focus on two spectral peaks, centered around 1470 cm^{-1} and 745 cm^{-1} . In the literature, the 1470 cm^{-1} peak arises from vibrations in the polymer backbone, and the 745 cm^{-1} peak arises from vibrations in the anion.^{18,19,24} The 1470 cm^{-1} peak obtained at different salt concentrations is shown in Fig. 1b, and the 745 cm^{-1} peak obtained at different salt concentrations is shown in Fig. 1c.

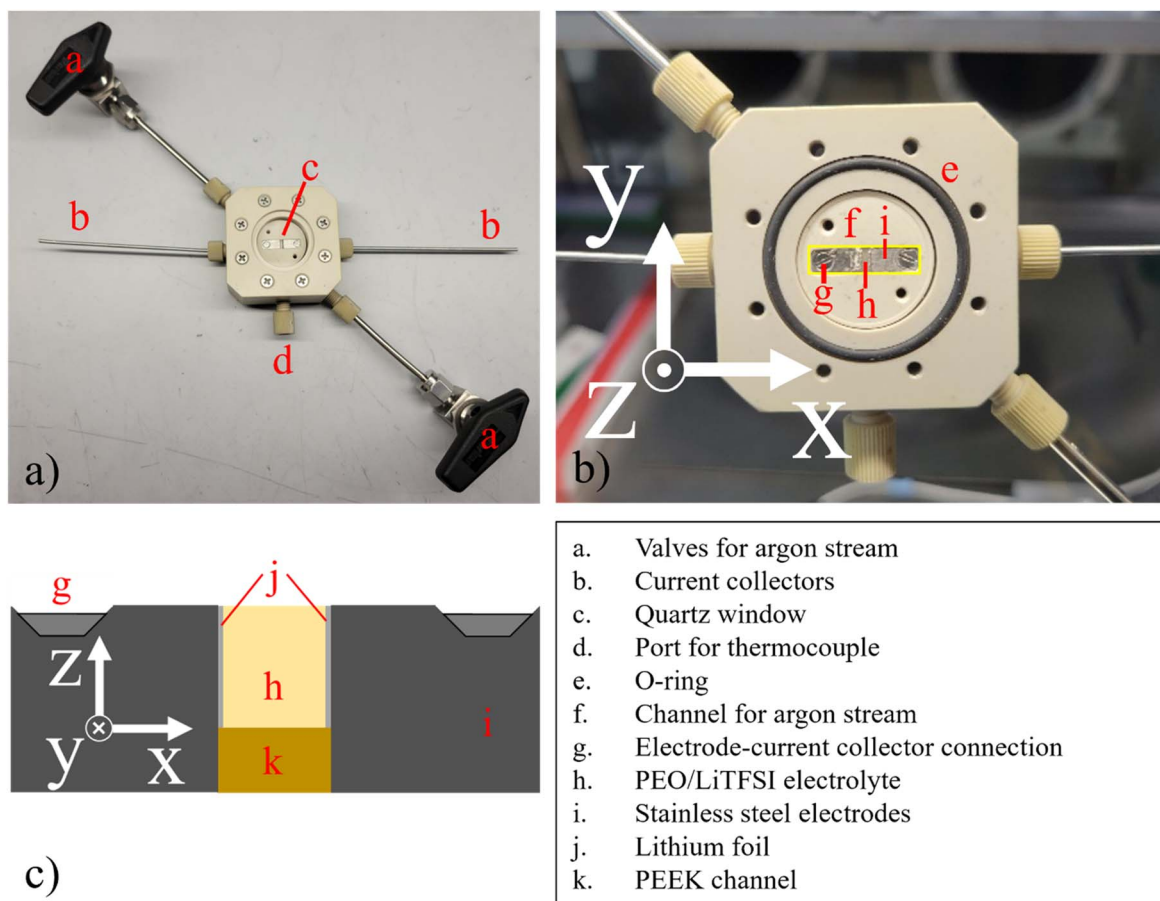


Figure 2. The electrochemical cell used for *operando* Raman spectroscopy. (a) View of entire cell from above. (b) Zoomed in view of the interior of the electrochemical cell with a yellow box around the experimental channel. (c) Diagram of the side view of the experimental channel.

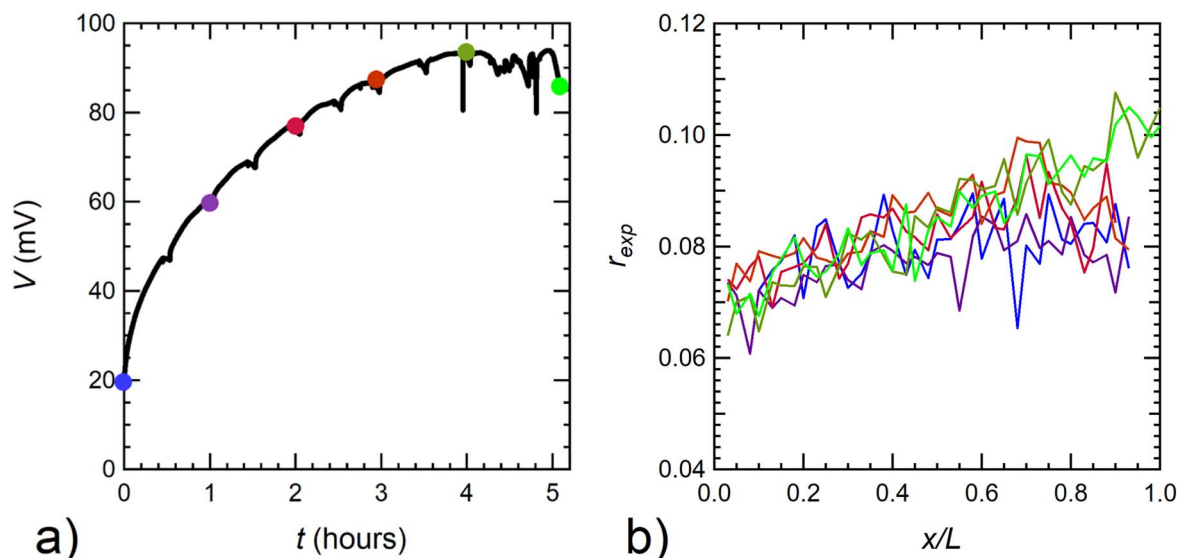


Figure 3. (a) Measured voltage as a function of time in the electrochemical cell during polarization, under an applied current density of 0.18 mA cm^{-2} . Colored circles correspond to time points at which salt concentration profiles were determined from *operando* Raman spectra. (b) Experimentally measured salt concentration, r_{exp} , as a function of normalized distance along the electrolyte, x/L , where $L = 1000 \mu\text{m}$. Colors indicate the time points at which the data were acquired and analyzed; see (a).

Figure 1b shows that the polymer backbone peak is a weak function of salt concentration. Figure 1c shows that the anion peak is strongly correlated with salt concentration. We define A_n to be the area under the anion peak normalized by the area under the polymer backbone peak.^{18,19} The spectral data were fit to pseudo-Voigt functions (1400 to 1520 cm^{-1} for the polymer backbone peak and 720 to 780 cm^{-1} for the anion peak), and the peak area was determined by analytical integration of the fitted functions. An example of our fitting procedure is provided in Fig. S3. A_n is plotted as a function of salt concentration r in Fig. 1d. A least squares linear fit through the data with the intercept held at 0 is represented by the dashed line in Fig. 1d, $A_n = 9.8r$. We use this equation as a calibration to determine local salt concentration from *operando* Raman spectra.

Measuring the Raman spectra of PEO/LiTFSI electrolytes (Fig. 1) is simple. However, obtaining Raman spectra in a polarized electrochemical cell required construction of a custom electrochemical cell. Most importantly, this cell required a transparent window through which the laser could pass, along with ensuring the electrodes and electrolyte remain air-free throughout the experiment. Figure 2 shows the electrochemical cell used in this study. The cell is made of polyether ether ketone (PEEK), and contains a channel used to flush argon through the cell during polarization, keeping it air-free. The channel holding the electrolyte and electrodes was machined separately from the base of the cell. This allowed for easy removal and cleaning between experiments. The channel holding the electrolyte is 0.1 cm thick (x -direction shown in Fig. 2), 0.4 cm long (y -direction), and 0.0875 cm deep (z -direction).

Polarization experiments were performed in a Li-PEO/LiTFSI-Li symmetric cell at current density $i = 0.18 \text{ mA cm}^{-2}$. This current density was found to be the upper limit of applied current densities that resulted in stable polarization without significant dendrite growth. In the interest of maximizing the magnitude of concentration gradients across the electrolyte, this upper limit of stable current was utilized. Using the values of κ , D , t_+^0 , and T_f we predict, using the methodology described in Refs. 10 and 11, that the limiting current density of this cell is 0.4 mA cm^{-2} . The current density used in this study lies well below the limiting current. The experiment was performed three times and data obtained from one experiment is shown in Fig. 3. Figure 3a shows the time dependence of the potential drop across the cell during polarization. Small changes in the measured voltage (typically 3 mV) occur at times when Raman spectra were measured. This indicates interference between the probe

and the sample—we have not identified the physical origin of the interference. As the time approaches 5 h , the voltage data begins to vary drastically over short periods of time. This voltage behavior is indicative of dendrite growth, and this was verified by noticeable dendrite formation after 4 h as shown by the optical micrograph of the cell in Fig. S4.^{10,27,28} Figure 3b shows the measured salt concentration as a function of position, x/L ($L = 0.1 \text{ cm}$), where the negative electrode is at $x/L = 0$ and the positive electrode is at $x/L = 1$, at selected times. These data reflect measured Raman spectra collected at 40 points separated by $25 \mu\text{m}$. The measured values of A_n were recast in terms of r using the calibration curve (Fig. 1d). The colors of the concentration profiles in Fig. 3b correspond with the colored markers in Fig. 3a which show the time points at which the concentration profiles were obtained. The time required for a single line scan was around 5 min which is small relative to the time scale required for significant changes in the local salt concentration profiles. After Raman measurements were recorded, micrographs were taken of the electrochemical channel. These micrographs were useful for observing dendrite growth within the cells. At early times we see the salt concentration oscillating around the average salt concentration value of $r_{\text{avg}} = 0.08$. As the cell is polarized, changes in concentration are most clearly seen at the positive electrode. It should be noted that while there was significant dendrite formation beginning after 4 h of polarization, the measured salt concentration gradients at 4 and 5 h essentially overlap, which would indicate a steady state has been reached within the electrolyte. This can also be inferred from the measured voltage as while there is oscillation in the voltage it remains relatively constant when compared to the change seen at earlier time periods.

We note that salt concentration measurements are challenging close to the lithium electrodes, and thus at times the salt concentration around $x/L = 0$ and $x/L = 1$ could not be measured reliably. For the data shown in Fig. 3, the relative position of the line scan was shifted $200 \mu\text{m}$ in the y -direction according to Fig. 2c between three and four hours to provide better data close to the electrodes. Due to the relatively small change in position of the line scan we do not expect that this change would result in any changes to the measured salt concentration compared to the previous position.

While the local salt concentration can vary during polarization, the average salt concentration must remain fixed at $r_{\text{avg}} = 0.08$. To check the validity of our measurements, the average salt concentration, r_{avg} , was calculated for each line scan. In Fig. 4 we plot δr

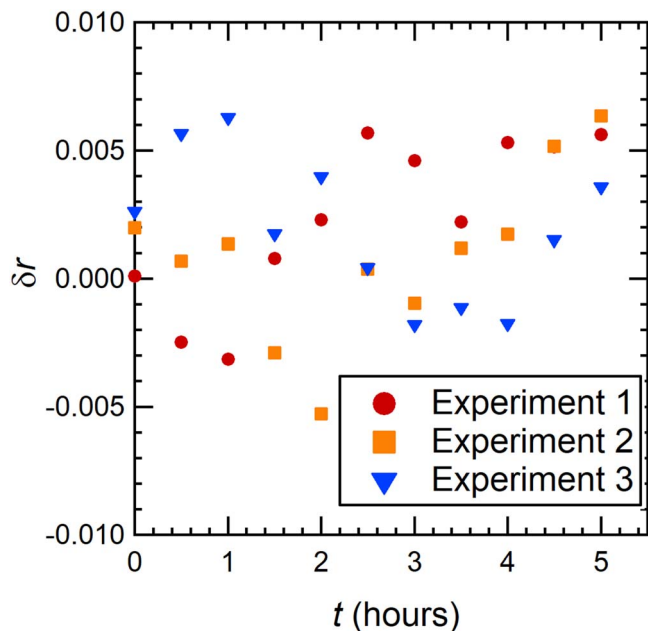


Figure 4. The deviation between the average salt concentration in the cell measured by *operando* Raman spectroscopy and the initial salt concentration (0.08), δr , as a function of polarization time for the 3 different experiments. In the absence of experimental error, we expect $\delta r = 0.08$.

($\delta r = r_{\text{avg}} - 0.08$) as a function of polarization time for all three experiments. The data in this figure are scattered around $\delta r = 0$, indicating that within experimental error the average salt concentration remains constant during polarization.

We are interested in understanding the difference between predicted salt concentration profiles and those that we measure using Raman spectroscopy. Figure 5a shows the steady state concentration profiles obtained from the three different experiments, $r = 0.08$ and $i = 0.18 \text{ mA cm}^{-2}$. For Experiment 1, measurements were made with 40 data points in a single line scan across the width of the electrolyte. For Experiments 2 and 3, 30 data points were taken over 3 different line scans separated by about $150 \mu\text{m}$ to

account for any variations that might be present within the electrolyte in the y -direction. For these experiments, the plotted data point represents the average for the 3 lines scans and the error bars correspond to the standard deviation of the 3 lines. Data from the three experiments are consistent with each other.

The solid curve in Fig. 5a is the predicted salt concentration profile utilizing methods developed by Pesko et al. and Frenck et al. which are based on concentrated solution theory.^{10,11} This prediction is made without resorting to any adjustable parameters. The steady state concentration profile, $r(x)$, is related to the current density and properties of the PEO/LiTFSI electrolyte. This relationship may be expressed as,

$$\int_{r(x=0)}^{r(x)} \frac{D(r)c(r)}{rt_{-}^0(r)} dr = \int_{r(x=0)}^{r(x)} \frac{\kappa}{\left(1 - \frac{1}{\rho_{+}}\right)(z_{+}v_{+})rF} \left(\frac{dU}{d\ln m}\right) = \int_{r(x=0)}^{r(x)} J(r) dr = -\frac{iL}{F} \left(\frac{x}{L}\right), \quad [1]$$

where $c(r)$ is the molar salt concentration, $t_{-}^0(r)$ is the transference number of the anion with respect to the solvent velocity, ρ_{+} is the current fraction, z_{+} is the charge of the cation, v_{+} is the number of cations produced when the salt dissociates, F is the Faraday constant, and $\frac{dU}{d\ln m}$ is the change in open circuit potential with respect to the natural log of molality. We utilized parameters measured for PEO/LiTFSI mixtures (PEO molecular weight of 275 kg mol^{-1}) reported in Ref. 29. Predicting salt concentration profiles only requires some of the parameters determined through full electrochemical characterization, and the parameters used in this work are reported in Table S1. The resulting expression $J(r)$ was fit to a 5th order polynomial,

$$J(r) = ar^5 + br^4 + cr^3 + dr^2 + er + f \left[\frac{\text{mol}}{\text{cm s}} \right], \quad [2]$$

with $a = 1.03\text{e-}4$, $b = -9.02\text{e-}5$, $c = 2.86\text{e-}5$, $d = -3.91\text{e-}6$, $e = 1.96\text{e-}7$, $f = 6.36\text{e-}10$. $r(x)$ is determined by using an initial guess of $r(x=0)$ and using Eq. 1 to solve for $r(x)$ where $0 \leq x \leq L$. Then r_{avg} is calculated, and if it does not match 0.08, a new $r(x=0)$ is chosen. This process is repeated iteratively until the $r_{\text{avg}} = 0.08$. The modeled concentration profile was fit to a polynomial,

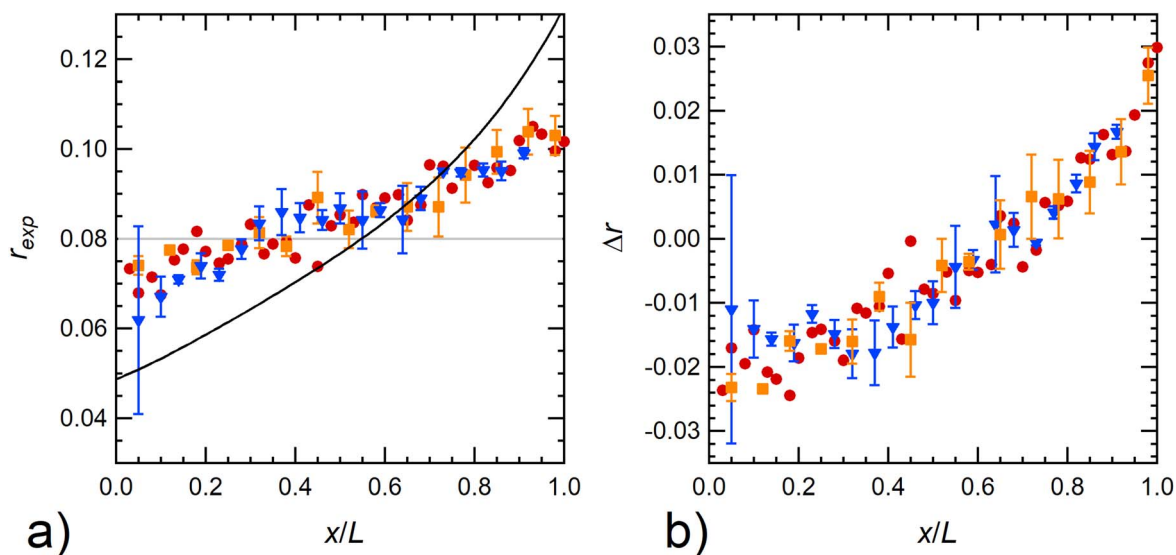


Figure 5. (a) Steady state salt concentration profiles of three independent experiments are plotted as a function of x/L . Three cells each with an r value of 0.08 were polarized using an applied current density of 0.18 mA cm^{-2} . The solid black line represents the theoretically predicted salt concentration profile, r_{theory} using concentrated solution theory. The solid gray line is indicative of the r_{avg} value of 0.08. (b) The difference in values of predicted and measured salt concentration as a function of x/L .

$$r_{\text{theory}} = 0.0807(x/L)^4 - 0.0982(x/L)^3 + 0.0596(x/L)^2 - 0.0407(x/L) + 0.0487 \quad [3]$$

The solid curve in Fig. 5a represents Eq. 3. Using these same procedures, the limiting current of an electrolyte can be predicted by determining the current density which results in a salt concentration of 0 at the negative electrode. For this experiment that value was found to be 0.4 mA cm^{-2} , which is well above the current density utilized in our experiments.

For an electrolyte with physical properties that are independent of salt concentration, the r versus x/L prediction would be a straight line. The curvature of the black line in Fig. 5a reflects the concentration dependence of transport and thermodynamic parameters of PEO/LiTFSI. The curvature is more pronounced near $x/L = 1$ (positive electrode) relative to $x/L = 0$ (negative electrode). At $x/L = 0$, the r_{theory} is 0.05, while that at $x/L = 1$ is 0.13. The departure of $r_{\text{theory}}(x)$ from 0.08 is thus highly asymmetrical: the departure at the positive electrode is about a factor of two smaller than that at the negative electrode. As can be seen in Fig. 5a, the asymmetrical departures from $r = 0.08$ are also observed in the experiments, but the magnitude of the departures are significantly smaller than the theoretical predictions. In addition, the dependence of r_{exp} on x/L exhibits less curvature than r_{theory} .

To better quantify the difference between theory and experiments, we define:

$$\Delta r = r_{\text{theory}} - r_{\text{exp}} \quad [4]$$

In Fig. 5b we plot Δr as a function of x/L . The values of Δr range from about -0.02 to $+0.02$.

We conclude this section by summarizing efforts in other studies to use *operando* Raman spectroscopy to measure salt concentration profiles in the presence of an applied current. In 1998 Rey et al. designed an optical cell, and demonstrated for the first time that Raman spectroscopy could be used to measure salt concentration profiles in a PEO electrolyte.¹⁹ In a subsequent paper, Georen et al. determined salt concentration profiles near the electrodes of a polarized symmetric cell with a statistical copolymer electrolyte comprising ethylene oxide and propylene oxide monomers (75 wt% ethylene oxide). They were specifically interested in understanding how concentration gradients develop close to the electrodes, and the experimental data were compared with theoretical predictions based on concentrated solution theory.²⁰ In this pioneering study, the authors found that the experimentally observed concentration polarization was less than that predicted by theory. However, the theory was based on transport and thermodynamic parameters which were assumed to be independent of salt concentration. In recent studies, Fawdon et al. measured concentration profiles by Raman spectroscopy, and used these measurements to backout the thermodynamic and transport parameters in liquid electrolytes. To our knowledge, Fig. 5 is the first comparison of salt concentration profiles measured with Raman spectroscopy and theoretical results, wherein the concentration dependence of transport and thermodynamic parameters used for the theoretical predictions was obtained from independent experiments.

Conclusions

We have measured salt concentration profiles in a model polymer electrolyte (PEO/LiTFSI) using *operando* Raman spectroscopy.

These measurements are compared with predicted salt concentration profiles based on concentrated solution theory. Our main conclusion is that concentration polarization is asymmetrical - the reduction of salt concentration near the negative electrode is smaller in magnitude than the increase of salt concentration near the positive electrode. This asymmetry arises from the concentration dependence of thermodynamic and transport parameters of PEO/LiTFSI.

Acknowledgments

This work was intellectually led by the Joint Center for Energy Storage Research (JCESR), an Energy Innovation Hub funded by the U.S. Department of Energy, Office of Science, Office of Basic Energy Science, under Contract No. DE-AC02-06CH11357, which supported work conducted by Z. J. H. under the supervision of N.P.B. Work at the Molecular Foundry was supported by the Office of Science, Office of Basic Energy Sciences, of the U.S. Department of Energy under Contract No. DE-AC02-05CH11231.

ORCID

Zach J. Hoffman <https://orcid.org/0000-0002-8989-8077>
 Michael D. Galluzzo <https://orcid.org/0000-0002-5776-0540>
 Madeleine P. Gordon <https://orcid.org/0000-0002-2818-7458>
 Jeffrey J. Urban <https://orcid.org/0000-0003-4909-2869>
 Nitash P. Balsara <https://orcid.org/0000-0002-0106-5565>

References

1. K. Xu, *Chem. Rev.*, **104**, 4303 (2004).
2. Q. Wang, L. Jiang, Y. Yu, and J. Sun, *Nano Energy*, **55**, 93 (2019).
3. S. Hess, M. Wohlfahrt-Mehrens, and M. Wachtler, *J. Electrochem. Soc.*, **162**, A3084 (2015).
4. C. Monroe and J. Newman, *J. Electrochem. Soc.*, **150**, A1377 (2003).
5. D. Aurbach, E. Zinigrad, Y. Cohen, and H. Teller, *Solid State Ionics*, **148**, 405 (2002).
6. J. B. Goodenough and Y. Kim, *Chem. Mater.*, **22**, 587 (2010).
7. C. Monroe and J. Newman, *J. Electrochem. Soc.*, **152**, A396 (2005).
8. Y. Choo, D. M. Halat, I. Villaluenga, K. Timachova, and N. P. Balsara, *Prog. Polym. Sci.*, **103**, 101220 (2020).
9. P. Barai et al., *J. Electrochem. Soc.*, **165**, A2654 (2018).
10. D. M. Pesko et al., *J. Electrochem. Soc.*, **165**, A3186 (2018).
11. L. Frenck et al., *Solid State Ionics*, **358**, 115517 (2020).
12. Y. Ma et al., *J. Electrochem. Soc.*, **142**, 1859 (1995).
13. J. Newman and K. E. Thomas-Alyea, *Electrochemical systems* (Wiley, Hoboken, New Jersey) 3rd ed. (2004).
14. Z. J. Hoffman, D. B. Shah, and N. P. Balsara, *Solid State Ionics*, **370**, 115751 (2021).
15. D. T. Hallinan and N. P. Balsara, *Annu. Rev. Mater. Res.*, **43**, 503 (2013).
16. D. Devaux, R. Bouchet, D. Glé, and R. Denoyel, "Mechanism of ion transport in PEO/LiTFSI complexes: Effect of temperature, molecular weight and end groups." *Solid State Ionics*, **227**, 119 (2012).
17. G. K. Sethi et al., *Solid State Ionics*, **368**, 115702 (2021).
18. J. Fawdon, J. Ihli, F. La Mantia, and M. Pasta, *Nat. Commun.*, **12**, 4053 (2021).
19. I. Rey, J. Bruneel, J. Grondin, L. Servant, and J. Lassègues, *J. Electrochem. Soc.*, **145**, 3034 (1998).
20. P. Georén, J. Adebahr, P. Jacobsson, and G. Lindbergh, *J. Electrochem. Soc.*, **149**, A1015 (2002).
21. Q. Cheng et al., *Nat. Commun.*, **9**, 1 (2018), <https://nature.com/articles/s41467-018-05289-z>.
22. J. D. Forster, S. J. Harris, and J. J. Urban, *J. Phys. Chem. Lett.*, **5**, 2007 (2014).
23. T. Yamanaka et al., *ChemSusChem*, **10**, 855 (2017).
24. J. Fawdon, G. J. Rees, F. La Mantia, and M. Pasta, *J. Phys. Chem. Lett.*, **13**, 27 (2022).
25. A. M. Tripathi, W. N. Su, and B. J. Hwang, *Chem. Soc. Rev.*, **47**, 736 (2018).
26. C. A. Lieber and A. Mahadevan-Jansen, *Appl. Spectrosc.*, **57**, 1363 (2003).
27. C. Brissot, M. Rosso, J. N. Chazalviel, and S. Lascaud, *J. Power Sources*, **81-82**, 925 (1999).
28. Y. Takeda, O. Yamamoto, and N. Imanishi, *Electrochemistry*, **84**, 210 (2016).
29. D. M. Pesko, S. Sawhney, J. Newman, and N. P. Balsara, *J. Electrochem. Soc.*, **165**, A3014 (2018).